Karol NAJDEK, Radosław NALEPA

Wroclaw University of Science and Technology

doi:10.15199/48.2019.11.61

Use of the D-decomposition technique for gains selection of the Dual Active Bridge converter output voltage regulator

***Abstract**. This article presents the Neimark's D-decomposition method for a PI compensator gains selection. The method has been used for the Dual Active Bridge converter output voltage regulator gains selection. The selection was basing on an experimentally identified transfer function. The obtained results were subjects to experimental verification. Elaborated mathematical and simulation models were also confirmed experimentally.*

***Streszczenie.** Niniejszy artykuł prezentuję zastosowanie metody D-rozbicia Neimarka podczas wyznaczania wartości wzmocnień regulatora PI. Metoda D-rozbicia została wykorzystana do wyznaczenia wzmocnień regulatora napięcia wyjściowego konwertera typu DAB w oparciu o jego eksperymentalnie zidentyfikowaną transmitancję. Uzyskane wyniki poddano weryfikacji eksperymentalnej. Zbudowany model matematyczny oraz symulacyjny zostały również potwierdzone na stanowisku eksperymentalnym.(**Zastosowanie metody D-rozbicia do wyznaczenia wzmocnień regulatora napięcia wyjściowego konwertera z podwójnym mostkiem aktywnym**)*

Keywords: Neimark's D-decomposition method, phase margin, gain margin, Dual Active Bridge, identification
Słowa kluczowe: D-rozbicie Neimarka, zapas fazy, zapas wzmocnienia, konwerter z podwójnym mostkiem aktywnym, identyfikacja

Introduction

Frequently used power electronics converters are still somehow challenging objects to control. This is not in terms of the control structure selection but rather in terms of the controller gains selection. Gains which guarantee stability of the unit in predefined operation range and also satisfactory dynamic performance. The operation range is to be understood here not only as power or voltage but also as operating temperature or components tolerance.

There is a number methods available for calculation of the gains in the continuous and the discrete domains [1, 2]. Nevertheless, the methods relay on numerous assumptions, simplifications and conversions. This sometimes does not reveal look of the complete set of stable solutions. The set from which one can choose intentionally subsets guaranteeing desired dynamic performance at certain stability margin. To overcome such limitation some rather non-standard techniques are to be used. One of them is the D-decomposition method proposed by Russian mathematician Yuri Isaakovich Neimark in 1948 [3]. The technique is relatively easy to use in the era of computers and is a subject to consideration in this article. The method determines asymptotically stable region (or regions if applicable) in space of parameters which can be the controller gains. Additionally, with some modifications it takes into account constrains related to desired phase and gain margins, PM and GM respectively [4].

The D-decomposition technique has been applied to gains selection of the Dual Active Bridge converter, DAB, output voltage PI regulator. The DAB topology, see Fig. 1, is commonly used in the electric power conversion chains where bidirectional power flow is required [5]. Mathematical derivation of the circuit transfer function for the control purpose is not straight forward. The model strongly depends on control scheme applied [6]. Therefore for purpose of this research the transfer function has been selected basing on a frequency domain identification method [7]. The identification has been conducted in the circuit under the Phase Shift Control scheme, PSC [8].
Obtained control results have been verified in mathematical, simulation and experimental ways. They are shown in this article.

This paper is organized as follows. Initially, a general description of Dual Active Bridge converter as the identification [7] and control [9] object is shown. After that, principles of the D-decomposition technique basing on a general example, without the computational and the measurement delays, are given. As next, effect of the delays on the calculation outcomes is discussed. This is followed by section with guidelines how to calculate the PI compensator gains with the gain and phase margins taken into account. In next section the presented mathematical apparatus is validated on the way of simulation and experiment. At the end conclusions are placed.

The DAB converter as the control object

The Dual Active Bridge converter, see Fig. 1, has been used as the control object. Its output voltage, $v_{\mathrm{DAB,out}}$, was controlled by means of a PI compensator.

The DAB converter consists of two H-bridge inverters. One on the primary side, dealing with the input Voltage, $v_{\mathrm{DAB,in}}$, and one on the secondary side, dealing with the $v_{\mathrm{DAB,out}}$, of a medium frequency transformer. The circuit has been chosen as a control object due to its popularity in the world of electric power processing. The popularity is driven by offered by the circuit features such as galvanic isolation by means of medium (or high) frequency transformer and bidirectional power flow control [5]. This makes it a good candidate to power electronics solutions used in energy storage systems [10], DC microgrids [11], aircraft applications [12] and many more. For purpose of this research a basic control method called Phase Shift Modulation [13, 14], PSM, has been used. It relies on fixed (set to 50%) duty cycle of the input and output H-bridges, $D_{\mathrm{in}} = D_{\mathrm{out}} = 0{,}5$. In such case the power transfer is controlled by means of phase shift, φ, in time between the input and output H-bridges. The phase varies in range $-\pi/2$ to $+\pi/2$ depending on transferred power level and direction. The basic control scheme may call for extension in order to compensate the dc-bias inductor current, especially when low on-state resistance MOSFET switches are used [9].

The test circuit used in this research relied on the basic control scheme and architecture with IGBT switches driven by PWM signal at frequency $f_s = 16$ kHz. The rated input and output voltages were $V_{\mathrm{DAB,in}}^{\mathrm{rtd}} = 60$ V and $V_{\mathrm{DAB,out}}^{\mathrm{rtd}} = 30$ V. More details about the circuit can be found in Table 1. Example experimentally recorded gate drive signals, inductor currents and voltages at different φ can be seen in Fig. 2.

Principles of the D-decomposition method

The method is also called the D-partition. Generally speaking, it establishes direct correlation between the characteristic equation phase and gain, and the space of permissible parameters for which the stability condition is met.

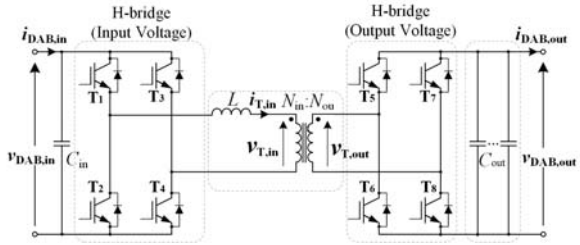

Fig. 1. General circuit diagram of the Dual Active Bridge converter

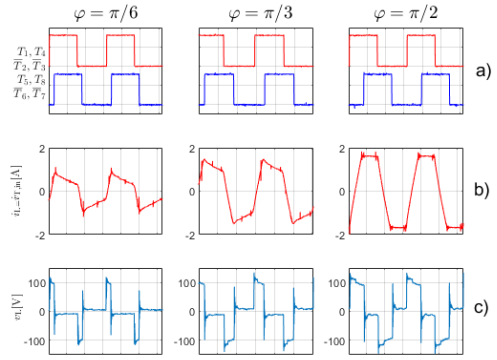

Fig. 2. Experimental visualization of the Phase Shift Modulation, PSM, control principle at three different phase shifts, φ: a) the gate drive signals of IGBT, b) the L inductance current, c) voltage across the L inductance

While considering nth-order characteristic equation, it is possible to signify a parametric surface $D(l, r = n - l)$, where l and r stand for number of the characteristic equation roots in the left and right half-plane respectively. If $l = n$ then there is no roots in the right half-plane, $r = 0$. In such condition the designated surface $D(l = n, 0)$ indicates stable region [3]. In order to calculate boundary of the stable region, it is necessary to substitute $s = j\omega$ in the characteristic equation, where $\omega = 2\pi f$ is a real number in range $-\infty < \omega < +\infty$. As next, the equation must be equated to zero. In fact, the real and imaginary parts are equated to zero. Solution of these equations leads to dependencies describing parametric hypersurface which precisely designates a boundary in the D surface. In this case, when $r = 0$, it is the stability boundary.

Once the stability boundary is known, it is necessary to find out which side is the stable area. This can be done using the original Neimark's guidelines [3]. For a single parameter it basically says that, while drawing the boundary of the parametric hypersurface (by changing frequency in direction from $-\infty$ to $+\infty$) then the left-hand side of the boundary is the stable region. It is the whole asymptotic stability region. For two changing (or tuneable) parameters ($m = 2$) additional boundary is needed. It can be achieved by introducing a ΔD_0 $(m-2)$-dimensional hyperplane [3]. The ΔD_0 hyperplane is related to the characteristic equation having a real zero at the origin of the s-plane ($s = 0$). Solving such relation leads to indication of complementary criterion for the second parameter region.

If particular gain margin, GM, and phase margin, PM, are to be applied then additional dedicated boundary must be found inside of the asymptotic stability region. It can be realized with the Shenton and Shafiei guidelines [15]. To do so, it is necessary to equate the characteristic equation to a complex number representing desired GM and PM, this instead of equating it to zero. In such case the formulated equation is called "relative characteristic equation", RCE, [15].

As an example, consider classical control structure in shown in Fig. 3.

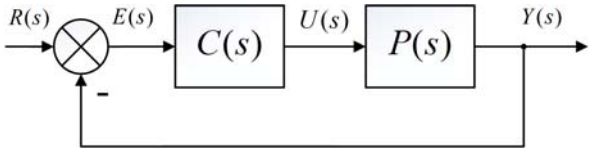

Fig. 3. Block diagram of an ideal closed-loop control structure, without signal transport and/or computational delays

The closed-loop transfer function of such system can be written in the Laplace domain as following:

$$G_{CL}(s) = \frac{Y(s)}{R(s)} = \frac{C(s)P(s)}{1 + C(s)P(s)} \tag{1}$$

where: $C(s)$ - the regulator transfer function; $P(s)$ – controlled plant transfer function; $R(s)$ - reference signal, $E(s)$ – the error, $U(s)$ – control signal; $Y(s)$ - the plant output. One should notice, that the $1 + C(s)P(s) = 0$ represents the characteristic equation. The $C(s)P(s)$ part stands for the open loop transfer function, $G_{OL}(s)$. Assume the plant transfer function as:

$$P(s) = \frac{Y(s)}{U(s)} = \frac{K}{sT_o + 1} \tag{2}$$

where: K is the steady state plant gain, and T_o is the plant time constant. The PI compensator transfer function can be written in form of:

$$C(s) = K_P + \frac{K_I}{s} \tag{3}$$

where K_P and K_I are the proportional and integral gains respectively. In such case the equation (1) can be rewritten:

$$G_{CL}(s) = \frac{K(sK_P + K_I)}{s^2 T_o + s(KK_P + 1) + KK_I} \tag{4}$$

where the denominator is the characteristic equation with the *-1* comprised inside.

The characteristic equation in general form, in the frequency domain, $s = j\omega$, can be written as a function with three arguments:

$$G_{OL}(j\omega, K_P, K_I) + 1 = 0 \tag{5}$$

or it can be rewritten in the well-recognised form used in the Nyquist plot analysis:

$$G_{OL}(j\omega, K_P, K_I) = -1 + j0 \tag{6}$$

where the $-1 + j0$ instead of -1 is written only to emphasize that the imaginary part exists but is equal to zero. Due to that the equation (6) can be split as following:

$$\Re\mathfrak{e}\left[G_{OL}(j\omega, K_P, K_I)\right] = -1 \tag{7}$$

$$\Im\mathfrak{m}\left[G_{OL}(j\omega, K_P, K_I)\right] = 0 \tag{8}$$

Solving the (7) and (8) for the K_P and K_I leads to:

(9) $$K_{\mathrm{P}} = -\frac{1}{K}$$

(10) $$K_{\mathrm{I}}(\omega) = \frac{\omega^2 T_{\mathrm{o}}}{K}$$

The equations (9) and (10) are describing the parametric hypersurface designating the stability boundary on the D surface. Plot of the equations with frequency as a parameter changing from $-\infty$ through 0 to $+\infty$ can be seen in Fig. 4. One can see that the left-hand side of the boundary, while moving with ω from $-\infty$ to 0, is the stable region. For the two parameters such boundary must be complemented by one more boundary driven by the ΔD_0 hyperplane. As mentioned before, it can be designated by comparison of the characteristic equation to 0 at the origin of the s-plane ($s = 0$). Basing on (4) it can be written:

(11) $$\Delta D_0 \Rightarrow K K_{\mathrm{I}} = 0$$

The equations (9)..(11) are completely describing the parametric hypersurface designating the stability boundary on the D surface.

The three selected points in Fig. 4 at frequencies $\omega_{1..3}$ are located exactly on the stability boundary as it can be also seen in corresponding Nyquist characteristics shown in Fig. 5. The three characteristics cross the $(-1, j0)$ point as expected while the gains are at the stability boundary.

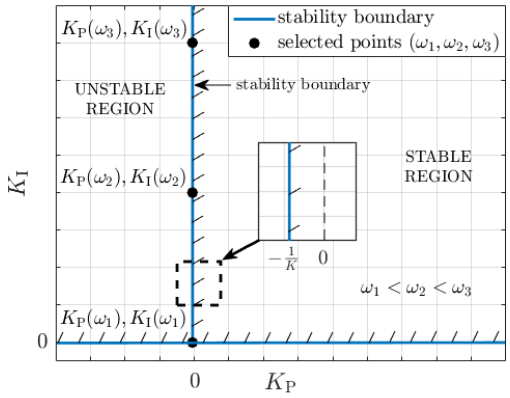

Fig. 4. Example of calculated global stability boundary of an ideal control structure shown in Fig. 3. It is calculated using the D-decomposition technique. The three points represent possible sets of K_{P} and K_{I} at different values of pulsation $\omega \in \{\omega_1, \omega_2, \omega_3\}$

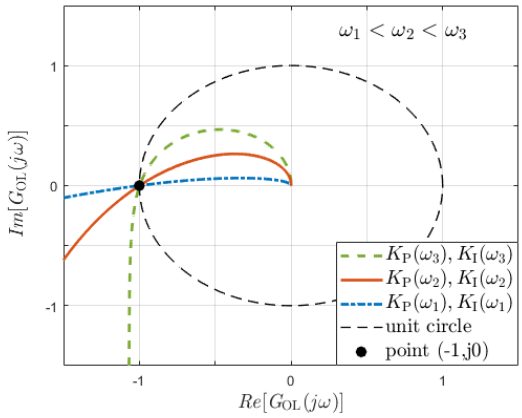

Fig. 5. The Nyquist plot for the three $\omega \in \{\omega_1, \omega_2, \omega_3\}$ from Fig. 4

D-decomposition technique for control structure with time delays

When it comes to the reality the control system model shown in Fig. 3 must be extended at least by time delays related to PWM effect, $\tau_{\mathrm{PWM}} = 1/16000\,s$, and miscellaneous signal conversion delays, $\tau_{\mathrm{A2D}} = 1/16000\,s$, see Fig. 6.

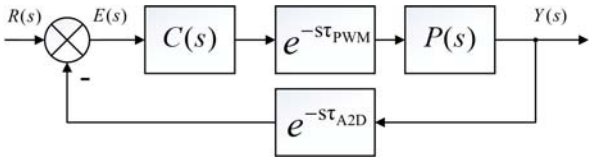

Fig. 6. Block diagram of closed loop control structure with the PWM and A2D delays

In such case the closed loop transfer function becomes:

(12) $$G_{\mathrm{CL}}(s) = \frac{C(s)e^{-s\tau_{\mathrm{PWM}}}P(s)}{1 + C(s)e^{-s(\tau_{\mathrm{PWM}}+\tau_{\mathrm{A2D}})}P(s)}$$

Following the same procedure as above, the K_{P} and K_{I} are now becoming functions of ω:

(13) $$K_{\mathrm{P}}(\omega) = \frac{-\cos\left((\tau_{\mathrm{PWM}} + \tau_{\mathrm{A2D}})\omega\right)}{K} + \frac{\omega T_{\mathrm{o}} \sin\left((\tau_{\mathrm{PWM}} + \tau_{\mathrm{A2D}})\omega\right)}{K}$$

(14) $$K_{\mathrm{I}}(\omega) = \omega\left(\frac{\omega T_{\mathrm{o}} \cos\left((\tau_{\mathrm{PWM}} + \tau_{\mathrm{A2D}})\omega\right)}{K} + \frac{\sin\left((\tau_{\mathrm{PWM}} + \tau_{\mathrm{A2D}})\omega\right)}{K}\right)$$

The equations (13) and (14) together with the (11) indicate new stable region for the gains as shown in Fig. 7. It can be seen that the delays have significant impact on the stable region. Now it is limited from the top when compared to the results from Fig. 4. In this case the three example points have different K_{P} too. Corresponding Nyquist plot can be seen in Fig. 8. The characteristics confirm that the gain points are at the edge of stability.

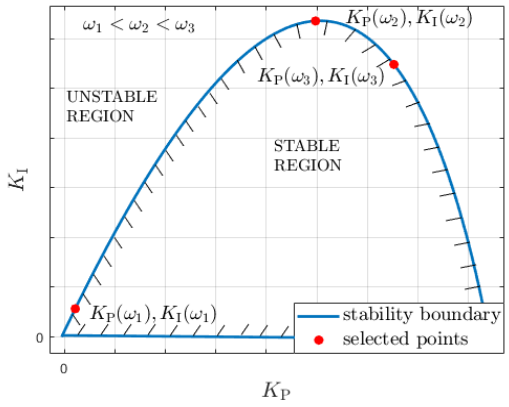

Fig. 7 Global stability boundary calculated using the D-decomposition technique. Inside is the stable region of controller gains K_{P} and K_{I}. The three example points are for different values of pulsation $\omega \in \{\omega_1, \omega_2, \omega_3\}$

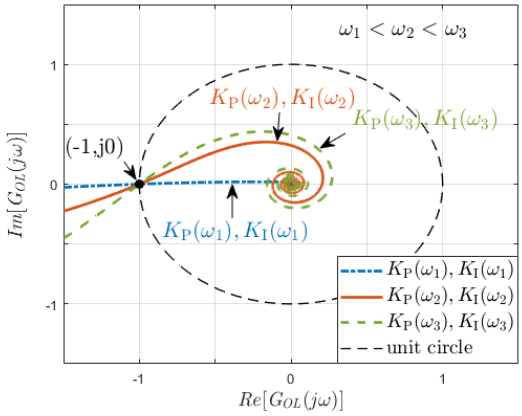

Fig. 8. The Nyquist plot for system with time delays as in Fig. 6. Three sets of gains K_P and $K_I$are shown for the same pulsation $\omega \in \{\omega_1, \omega_2, \omega_3\}$ as in Fig. 7

The gain and phase margins combined with the D-decomposition technique

For practical reasons certain gain and phase margins, GM and PM, must be guaranteed in every control structure [4]. This can be achieved with the D-decomposition technique too [15]. The equation (6) must be now extended by a part allowing incorporation of additional limits. To do so, the point $(-1, j0)$ must be shifted into a different location on the unity circle of the Nyquist plot. The new location must reflect desired GM at corresponding PM (or vice versa) in the polar plane [16]. It can be written in generalized form as following:

$$G_{\mathrm{OL}}\left(j\omega, K_{\mathrm{P}}, K_{\mathrm{I}}\right) = a + jb \tag{15}$$

where $a + jb$ stand for coordinates of an arbitrary point in the polar plane.

The relation between the PM and GM in graphical form can be seen in Fig. 9. The Fig. 9a concerns the GM representation in terms of the real and imaginary parts of the complex number. Taking into account that the GM is expressed in decibels, dB, it can be written:

$$\begin{aligned} a_{\mathrm{GM}} &= -10^{\left(-\mathrm{GM}/20\right)} \\ b_{\mathrm{GM}} &= 0. \end{aligned} \tag{16}$$

If the PM in radians, rad , is considered, see Fig. 9b, the real and imaginary parts become:

$$\begin{aligned} a_{\mathrm{PM}} &= \cos(\mathrm{PM} + \pi) \\ b_{\mathrm{PM}} &= \sin(\mathrm{PM} + \pi) \end{aligned} \tag{17}$$

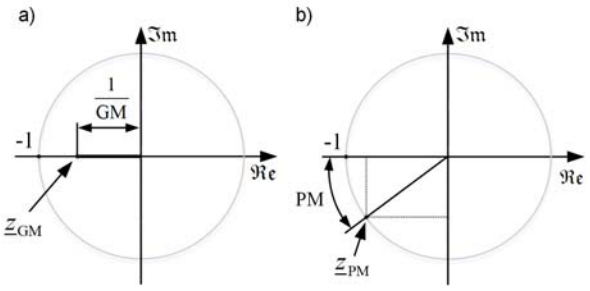

Fig. 9. Graphical representation of: a) the Gain Margin, GM, and b) the Phase Margin, PM, in the Nyquist plot. They can be represented by complex numbers $\underline{z}_{\mathrm{GM}} = a_{\mathrm{GM}} + jb_{\mathrm{GM}}$ and $\underline{z}_{\mathrm{PM}} = a_{\mathrm{PM}} + jb_{\mathrm{PM}}$ corresponding to certain the GM and PM respectively

Basing on equations (15) and (16) the K_{P} and K_{I} gains for required GM can be written as following:

$$\begin{aligned} K_{\mathrm{P}}\left(\omega, \mathrm{GM}\right) = 10^{-\mathrm{GM}/20}\Bigg(& \frac{-\cos\left(\left(\tau_{\mathrm{PWM}} + \tau_{\mathrm{A2D}}\right)\omega\right)}{K} \\ & + \frac{\omega T_{\mathrm{o}} \sin\left(\left(\tau_{\mathrm{PWM}} + \tau_{\mathrm{A2D}}\right)\omega\right)}{K}\Bigg) \end{aligned} \tag{18}$$

$$\begin{aligned} K_{\mathrm{I}}\left(\omega, \mathrm{GM}\right) = 10^{-\mathrm{GM}/20}\omega\Bigg(& \frac{\omega T_{\mathrm{o}} \cos\left(\left(\tau_{\mathrm{PWM}} + \tau_{\mathrm{A2D}}\right)\omega\right)}{K} \\ & + \frac{\sin\left(\left(\tau_{\mathrm{PWM}} + \tau_{\mathrm{A2D}}\right)\omega\right)}{K}\Bigg) \end{aligned} \tag{19}$$

Similarly, basing on (15) and (17), from the PM the K_{P} and K_{I} become:

$$\begin{aligned} K_{\mathrm{P}}\left(\omega, \mathrm{PM}\right) = & \frac{-\cos\left(\mathrm{PM} + \left(\tau_{\mathrm{PWM}} + \tau_{\mathrm{A2D}}\right)\omega\right)}{K} \\ & + \frac{\omega T_{\mathrm{o}} \sin\left(\mathrm{PM} + \left(\tau_{\mathrm{PWM}} + \tau_{\mathrm{A2D}}\right)\omega\right)}{K} \end{aligned} \tag{20}$$

$$\begin{aligned} K_{\mathrm{I}}\left(\omega, \mathrm{PM}\right) = \omega\Bigg(& \frac{\omega T_{\mathrm{o}} \cos\left(\mathrm{PM} + \left(\tau_{\mathrm{PWM}} + \tau_{\mathrm{A2D}}\right)\omega\right)}{K} \\ & + \frac{\sin\left(\mathrm{PM} + \left(\tau_{\mathrm{PWM}} + \tau_{\mathrm{A2D}}\right)\omega\right)}{K}\Bigg) \end{aligned} \tag{21}$$

Visualizing plots corresponding to equations (18)..(21) together with (13), (14) and (11) can be seen in Fig. 10. The cross point of the gains functions (depending on the ω, GM and PM) stands for desired GM and PM.

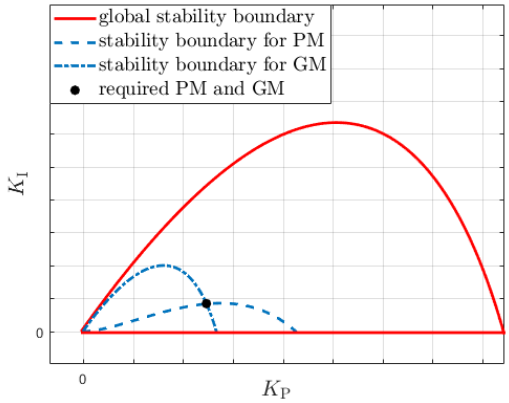

Fig. 10. The Global stability boundary for control system with time delays as shown in Fig. 6, together with stability boundary for the PM and GM. The intersection of the PM and GM curves indicates the requested margins

Experimental and simulation results for the DAB converter

The equations (11) and (18)..(21) can be used to indicate the proportional and integral gains in combination with a plant transfer function in form of (2). In case of the DAB converter such control-to-output transfer function can be found by means of an identification [7]. For purpose of this research it was estimated as $P_{\mathrm{DAB}}^{\mathrm{exp,est,c2o}}(s)$ basing on laboratory measurement, $P_{\mathrm{DAB}}^{\mathrm{exp,m,c2o}}(s)$, of the Bode characteristics shown in Fig. 11. The gain and phase were measured in frequency range of 0,1 Hz to 4 kHz.

(22) $$P_{\mathrm{DAB}}^{\mathrm{exp,est,c2o}}(s)=\frac{46,4}{s\,0,021+1}$$

The estimated transfer function was further verified by comparison of its step response with responses from the experimental circuit and detailed simulation model built in Simulink, see Fig. 12. Obtained results confirm correctness of the estimation.

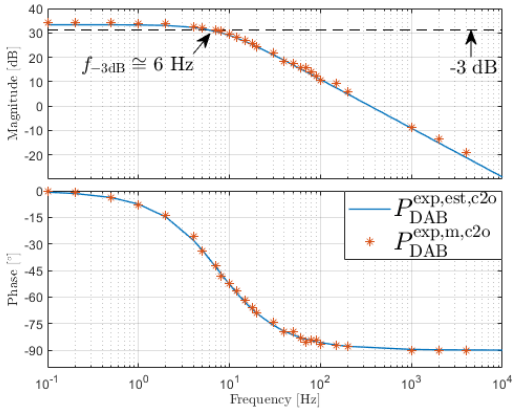

Fig. 11. The Bode plots of control-to-output transfer function basing on experimentally measured data points, $P_{\mathrm{DAB}}^{\mathrm{exp,m,c2o}}$, and estimated equation (22), $P_{\mathrm{DAB}}^{\mathrm{exp,est,c2o}}$. The measurements were done at the converter rated power

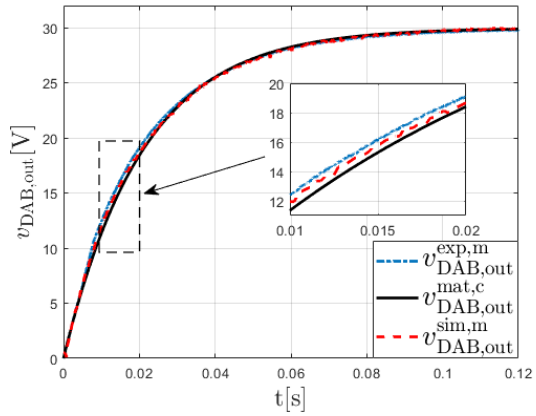

Fig. 12. Step responses of (control-to-output) DAB converter output voltages: experimentally measured, $v_{\mathrm{DAB}}^{\mathrm{exp,m}}$, mathematically calculated, $v_{\mathrm{DAB}}^{\mathrm{mat,c}}$, and simulated, $v_{\mathrm{DAB}}^{\mathrm{sim,m}}$. Measured at the phase shift reference step command of φ = 0,646 rad, with 16 kHz sampling rate

In next step the $P_{\mathrm{DAB}}^{\mathrm{exp,est,c2o}}(s)$ was used for the K_{P} and K_{I} gains selection – this with the GM = 40 dB and PM = 80º. The K_{P} = 0,04 rad/V and K_{I} = 4,6 rad/V·s were selected. Results according to the closed loop control structure from Fig. 6 can be seen in Fig. 13. The results are for changing reference of the output voltage, $V_{\mathrm{DAB,out}}^{\mathrm{ref}}$, at the rated load of 100 W. Initially the $V_{\mathrm{DAB,out}}^{\mathrm{ref}}$ changed from 20 V to $V_{\mathrm{DAB,out}}^{\mathrm{rtd}}$ = 30 V. Later the $V_{\mathrm{DAB,out}}^{\mathrm{ref}}$ varied within the ±10 % voltage tolerance envelope. Obtained results confirm usefulness of the D-decomposition method in selection if the compensator gains. The results from simulation and mathematical modelling are not exactly the same as experimental results but within acceptable tolerance. It is mainly a matter of compromise on the circuit parasitic components not reflected in modelling.

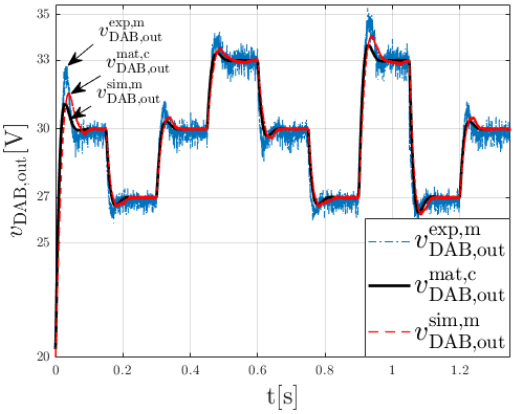

Fig. 13. The DAB converter output voltage, $v_{\mathrm{DAB,out}}$, regulation results (experimental, simulation and mathematical) with closed loop control structure shown in Fig. 6. The results have been recorded at the output rated power $P_{\mathrm{DAB,out}}^{\mathrm{rtd}}$ = 100 W and switching frequency of 16 kHz. The K_{P} = 0,04 rad/V and K_{I} = 4,6 rad/V·s were selected basing on the identified transfer function (22) and the D-decomposition technique

Conclusion/Summary

The Neimark's D-decomposition technique has been recalled to select the DAB converter output voltage compensator gains. The D-decomposition has been applied in conjunction with experimentally identified control-to-output converter transfer function.

Obtained experimental, simulation and mathematical results have proven that such approach can guarantee relatively easy selection of control settings in advanced power electronics equipment.

Further research will be carried on the control object parameters variation in presence of selected control parameters.

Tables

Table 1. Parameters of the DAB circuit

Parameter Name	Value
Input rated voltage, $V_{\mathrm{DAB,in}}^{\mathrm{rtd}}$	60 VDC
Output rated voltage, $V_{\mathrm{DAB,out}}^{\mathrm{rtd}}$	30 VDC
Output rated power, $P_{\mathrm{DAB,out}}^{\mathrm{rtd}}$	100 W
Output voltage tolerance, $V_{\mathrm{DAB,out}}^{\mathrm{tol}}$	±10 %
Converter inductance, L	140 µH
Input capacitance, C_{in}	4 mF
Output capacitance, C_{out}	4 mF
Transformer turn ratio, n	2
Switching frequency, f_{s}	6 kHz 16 kHz
Assumed efficiency, η_{DAB}	80 %
Gate drive dead time, T_{dt}	1µs

Table 2. The DAB output voltage regulator gains

Parameter Name	Value
Proportional gain, K_{P}	0,04 rad/V
Integral gain, K_{I}	4,6 rad/V·s

Acknowledgment

The authors of this paper wish to thank Dr Marcin Zygmanowski for inspiring discussions in the field of practical power electronics supported by laboratory experiments.

***Authors**: mgr inż. Karol Najdek, Politechnika Wrocławska, Wydział Elektryczny, Katedra Energoelektryki, Wybrzeże Wyspiańskiego 27, 50-370 Wrocław, E-mail: karol.najdek@pwr.edu.pl; dr inż. Radosław Nalepa, Politechnika Wrocławska, Wydział Elektryczny,*

Katedra Energoelektryki, Wybrzeże Wyspiańskiego 27, 50-370 Wrocław, E-mail: radoslaw.nalepa@pwr.edu.pl.

REFERENCES

[1] Ogata K., Modern Control Engineering, 5th Edition, *Prentice Hall*, (2002)
[2] Franklin G. F. and Powell J. D., Digital control of dynamic systems, *Addison-Wesly Publishing Company,* (1980)
[3] Niejmark J.I., Ob opriedielenji znaczenij paramietrow, pri kotorych sistiema awtomaticzeskogo riegulirowanja ustojczziwa, *Awtomatika i Telemiechanika*, (1948), vol. 3
[4] Chang C.-H., Han K.-W., Gain margins and phase margins for control systems with adjustable parameters, *Journal of Guidance, Control, and Dynamics*, (1989), vol. 13, no. 3, 404-408
[5] Doncker R. W. A. A. D., Divan D. M., and Kheraluwala M. H., A three-phase soft-switched high-power-density DC/DC converter for high-power applications, *IEEE Transactions on Industry Applications*, (1991), vol. 27, no. 1, 63-73.
[6] Kayaalp I., Demirdelen T., Koroglu T., Cuma M. U., Bayindir K. C., Tumay M., Comparison of Different Phase-Shift Control Methods at Isolated Bidirectional DC-DC Converter, *International Journal of Applied Mathematics, Electronics and Computers*, (2016), vol. 4, no. 3, 68
[7] Najdek K., Nalepa R., Zygmanowski M., Identification of Dual-Active-Bridge converter transfer function, *Przegląd Elektrotechniczny*, (2019), vol. 3, 151–154
[8] Ling S., Wanjun L., Jun H., Zhuoqiang L., Yao C., Yue W., Full discrete-time modeling and stability analysis of the digital controlled dual active bridge converter, *International Power Electronics and Motion Control Conference*, (2016), 3813-3817
[9] Nalepa R., Zygmanowski M., Michalik J., Dual-Active-Bridge converter inductance DC-bias current compensation under low and high load conditions, *Przegląd Elektrotechniczny*, (2018), no. 07, 1-5
[10] Saeed S., Design and construction of a DAB Converter for integration of energy storage systems in Power Electronic applications, *The 6th International Conference on Power Electronics Systems and Applications*, (2015), 1–7
[11] Mo Q. Ye, R., Li H., Impedance modeling and verification of a dual active bridge (DAB) DC/DC converter enabled DC microgrid in FREEDM system, *International Power Electronics and Motion Control Conference*, (2016), 2875–2879
[12] Pizzo A. D., Model A. S., Model-Reference Adaptive Control of a Dual Active Bridge dc-dc Converter for Aircraft Applications, *International Symposium on Power Electronics, Electrical Drives, Automation and Motion,* (2018), pp. 502–506, 2018.
[13] Qin H., Kimball J. W., Generalized average modeling of dual active bridge DC-DC converter, *IEEE Transactions on Power Electronics*, (2012), vol. 27, no. 4, 2078–2084
[14] Nguyen T. L., Griepentrog G., Phung V. T., Modeling and control of dual active bridge converter with two control loops and output filter, *The 43rd Annual Conference of the IEEE Industrial Electronics Society*, (2017), 4683–4689
[15] Shenton A. T., Shafiei Z., Relative Stability for Control Systems with Adjustable Parameters, (1994), vol. 17, no. 2, 304–310
[15] Jinggong L., Yali X., Donghai L., Calculation of PI Controller Stable Region Based on D-Partition Method, (2010), no. 2, 2185-2189